Available online at www.sciencedirect.com

ScienceDirect

Proceedings of the Combustion Institute 38 (2021) 5281–5288

Proceedings of the Combustion Institute

www.elsevier.com/locate/proci

Interaction mechanism among CO, H_2S and CuO oxygen carrier in chemical looping combustion: A density functional theory calculation study

Chaohe Zheng, Haibo Zhao*

State Key Laboratory of Coal Combustion, School of Energy and Power Engineering, Huazhong University of Science and Technology, Wuhan 430074, PR China

Received 8 November 2019; accepted 9 June 2020
Available online 30 August 2020

Abstract

When using coal-derived syngas or coal as fuel in chemical looping combustion (CLC), CO as a representative pyrolysis/gasification product and H_2S as the main sulfurous gas coexist in fuel reactor. Either CO or H_2S can absorb on the surface of CuO (the active component of Cu-based oxygen carriers), and reactions will occur among them. In this study, density functional theory (DFT) calculations are conducted to investigate the interaction among H_2S, CO, and CuO, including: the reaction between CO and H_2S over CuO particle, the influence of CO on the H_2S dissociation and further reaction process, and the impact of H_2S dissociation products on CO oxidation. Firstly, the co-adsorption results suggest that H_2S might directly react with CO to produce COS via the Eley–Rideal mechanism, while CO prefers to react with HS* or S* via the Langmuir–Hinshelwood mechanism. This means that the reaction mechanisms between CO and H_2S will change as the H_2S dissociation proceeds, which has already been forecasted by the co-adsorption energies and verified by all of potential Eley–Rideal and Langmuir–Hinshelwood reaction pathways. Then, the influence of CO on the H_2S dissociation process is examined, and it is noted that the presence of CO greatly limits the dissociation of H_2S due to the increased energy barrier of the rate-determining dehydrogenation step. Furthermore, the impact of H_2S dissociation products on CO oxidation by CuO is also investigated. The presence of H_2S and S* significantly supresses the CO oxidation activity, while the presence of HS* slightly promotes the CO oxidation activity. Finally, the complete interaction mechanisms among H_2S, CO, and CuO are concluded. It should be noted that COS will be inevitably produced via the Langmuir–Hinshelwood reaction between surface S* and CO*, which is prior to H_2O generation and subsequent sulfidation reaction.

Keywords: Chemical looping combustion; CO and H_2S; Density functional theory; Interaction mechanism

1. Introduction

Chemical looping combustion (CLC), with the characteristics of inherent CO_2 separation during fossil fuel conversion process, has been proposed

* Corresponding author.
E-mail address: hzhao@mail.hust.edu.cn (H. Zhao).

https://doi.org/10.1016/j.proci.2020.06.260

as one of the most promising technologies to address the global warming issue [1,2]. Typically, there are two reactors in the chemical looping system, *i.e.* fuel reactor and air reactor. Oxygen carrier (OC), as the medium to bridge the two reactors, is regarded as a key issue in CLC. Cu-based materials have been extensively investigated as suitable OCs, due to the excellent reactivity and high oxygen transport capacity [3]. Nevertheless, Cu-based OC has been demonstrated as a sulfur-sensitive material, which is easily to be contaminated by sulfur-containing species and thus resulting in degraded reaction performance (reactivity, durability, and resistance to sintering/agglomeration).

H_2S and CO always coexist in fuel reactor when using natural gas, biogas, coal-derived syngas, or coal (H_2S as main sulfur species released from coal pyrolysis) as fuels [4]. Recently, extensive research on the performance of Cu-based OC with sulfur-containing syngas has been evaluated in CLC [5–9], and a high concentration of COS has been detected from the exhaust [8,9]. Wang et al. [9] conjectured that, in the CLC atmosphere (with copper ore as OC), the COS formation might be via the reactions between SO_2 or H_2S and CO. Over the ZnO or Fe_2O_3 surface, the formation of COS from the mixture of $CO/CO_2/H_2S$ may occur, which was also verified by experiments [10-12]. Through density functional theory (DFT) calculations, Ling et al. [13] further found that the formation of COS from the CO–H_2S reaction over the ZnO surface was easier than that between CO_2 and H_2S.

To date, three different mechanisms have been reported for the interaction of two gaseous species over sorbent surface, including the Mars-van Krevelen (MvK) mechanism, the Eley-Rideal (E-R) mechanism, and the Langmuir-Hinshelwood (L-H) mechanism [14]. The E-R mechanism represents the gas-solid heterogeneous reaction, and the L-H mechanism signifies the homogeneous reaction between two adsorbed molecules. In a previous study, Ling et al. [13] speculated that COS was entirely produced via the L-H reaction between the dissociated S* and adsorbed CO*. However, the concentration of CO in fuel reactor was more than two orders of magnitude higher than that of H_2S, indicating a high possibility of the E-R mechanism for the real heterogeneous reaction, which was rarely investigated.

On the other side, the presence of CO might influence the H_2S adsorption on the CuO surface and further reaction with CuO, and *vice versa*. Recently, DFT calculations have been successfully conducted to explore the microscopic adsorption mechanisms of CO [15,16] or H_2S (resultant HS* and S*) [17,18] on the surface of CuO (111). These species are all strongly chemisorbed at the same copper site on the CuO surface, indicating a competitive adsorption process. Therefore, when H_2S and CO coexist on the surface of CuO, there must be mutual effect between them for the competitive adsorption. To be more specific, the H_2S adsorption, dissociation, and further reaction with CuO might be affected by the presence of CO, and CO oxidation would be influenced by H_2S as well. Nevertheless, there is no report on the intrinsic interactions of CO or H_2S with CuO (neither of the homogeneous or heterogeneous reactions among two species). Therefore, gaining fundamental insights into the detailed interaction among the system of H_2S, CO, and Cu-based OC is highly desired.

In this study, DFT calculations are conducted to reveal the interaction mechanism among H_2S, CO, and CuO. As known, there are three distinct stages during the H_2S dissociation process (*i.e.*, H_2S, HS*+H*, and S*+2H*) [17,18]. Thus, in this work, the co-adsorptions of CO and H_2S, HS*+H*, S*+2H* are firstly investigated respectively, aiming to preliminarily determine the interaction mechanism. Then, DFT calculations are carried out to examine all the possible reaction pathways (via either the L-H or E-R mechanism). Next, the influence of CO on the H_2S dissociation process and subsequent sulfidation reaction, as well as the impact of H_2S dissociation products on CO oxidation are also investigated. Finally, the entire schematic of reaction pathways is obtained. Based on the energy barriers analysis, the rate-limiting steps are determined. These fundamental insights can benefit the acquisition of the intrinsic interaction and reaction mechanism/kinetics of H_2S or CO over Cu-based OC, and provide useful guidance to the design of robust OCs used in a realistic chemical-looping system.

2. Computational details

All DFT calculations in this study are conducted by the CASTEP (Cambridge Serial Total Energy Package) program package. The generalized gradient approximation (GGA) in the form of Perdew-Wang (PW91) is chosen for the electron exchange-correlation energy [19]. The interactions of electrons and ions are modeled by ultrasoft pseudo-potential. The cutoff energy of 400 eV is adopted. The Brillouin zone interactions are described within the Monkhorst-Pack type mesh of $5 \times 7 \times 5$ and $3 \times 2 \times 1$ for CuO bulk cell and CuO slab, respectively. The GGA+U method is adopted to describe the strong electron correlations of transition metals, and 7.5 eV is selected, as it is a reasonable U value for the Cu 3d orbitals [20,21]. The van der Waals-inclusive correction (DFT-D) with the Ortmann–Bechstedt–Schmidt (OBS) method is applied, and the convergence criteria for total energy, maximum inter-atomic force, and displacement are 1.0×10^{-5} eV/atom, 0.03 eV/Å, and 0.001 Å, respectively.

As shown in Fig. 1a, the lattice parameters of the CuO unit cell ($a = 4.653$ Å, $b = 3.410$ Å,

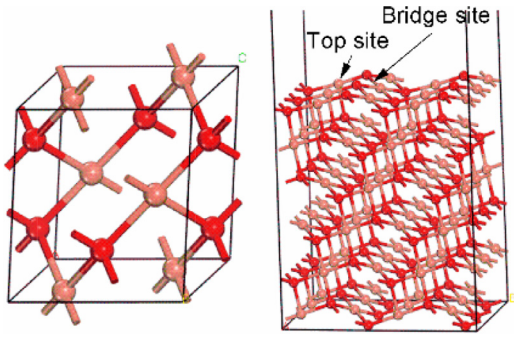

Fig. 1. (a) CuO unit cell; (b) six-layer CuO (111) slab.

$c = 5.108$ Å, and $\beta = 99.50°$) are in good agreement with the experimental values ($a = 4.682$ Å, $b = 3.424$ Å, $c = 5.127$ Å, and $\beta = 99.42°$) [22]. Consequently, a six-layer p (2×3) CuO (111) slab model is constructed and shown in Fig. 1b, in which the top three layers are allowed to relax and the bottom three layers are fixed. The vacuum space of 15 Å is added perpendicular above the surface. More computational details and verifications can refer to Section S1 in Supplemental Material (SM).

In order to investigate the interactions between gaseous species and bare slab, the adsorption energy, E_{ads}, is defined as $E_{ads} = E(A) + E(B) - E(AB)$, where $E(AB)$ is the total energy of the adsorption structure; $E(A)$ and $E(B)$ represent the total energies of substrate and adsorbate, respectively. Moreover, the complete LST/QST (linear/quadratic synchronous transit) approach is used to calculate the energy barrier, E_b, which is defined as: $E_b = E(TS) - E(IS)$, where $E(TS)$ and $E(IS)$ are the energies of the transition state and the initial state, respectively.

3. Results and analysis

3.1. Co-adsorption of H_2S and CO on the CuO (111) surface

To find the potential co-adsorption configurations of H_2S and CO, the individual adsorption of CO or H_2S (including the dissociated HS* and S*) on the CuO (111) surface is firstly investigated, and all possible active adsorption sites are considered (see Section S2 in SM). As listed in Table 1, the adsorption energies of CO and H_2S are 65.65 and 88.35 kJ/mol, respectively, which are consistent with the literature results [15,18]. Both H_2S and CO are intensively chemisorbed at the same site of T_{Cu3f}. The higher adsorption energy of H_2S (or HS*, S*) than that of CO indicates that H_2S (or HS*, S*) preferentially adsorbs on the surface of CuO (111) in the competitive adsorption process.

Table 1
The adsorption energies (E_{ads}/kJ·mol^{-1}) of single adsorption and co-adsorption.

	single	CO, H_2S	CO, HS*	CO, S*
CO	65.65	63.99	76.43	69.42
H_2S	88.35	86.69	–	–
HS*	203.80	–	197.11	–
S*	218.98	–	–	212.70

The configurations in Fig. 2 represent the co-adsorptions between H_2S (as well as HS*, S*) and CO. As listed in Table 1, the adsorption energy of CO in the presence of H_2S (Fig. 2a) is 63.99 kJ/mol, which is slightly lower than that of the individual adsorption energy of CO (65.65 kJ/mol), implying that the presence of H_2S weakens the adsorption of CO. As known, H_2S is preferentially adsorbed on the surface, and CO might be inclined to exist in the form of the gas state to react with the adsorbed H_2S*. It is therefore inferred that the interaction between CO and H_2S might follow the E-R mechanism via the reaction of $H_2S^* + CO_{(g)} \rightarrow COS_{(g)} + 2H^*$, where '*' represents the adsorbed state and '(g)' represents gas state. On the other side, the higher adsorption energies of CO in the presence of HS* or S* (76.43 or 69.42 kJ/mol, in Table 1) indicate that the adsorption of CO would be enhanced. Since HS* and S* species are preferentially adsorbed on the surface as well, CO might first absorb on the CuO surface and then react with the adsorbed HS* and S* species via the L-H reactions of $HS^* + CO^* \rightarrow COS^* + H^*$ and $S^* + CO^* \rightarrow COS^*$. In other words, the reaction mechanisms of H_2S and CO would change as the H_2S dissociation proceeds.

3.2. The reaction between CO and H_2S on the surface of CuO

To further determine the CO/H_2S reaction mechanism over the CuO surface, all of the possible interaction routes are then considered. The configurations in Fig. 3 represent CO adsorbs on the H_2S (or HS*, S*) pre-adsorbed CuO surface. Following the E-R mechanism, H_2S (or HS*, S*) is pre-adsorbed on the CuO surface, and the corresponding reaction routes are: $H_2S^* + CO_{(g)} \rightarrow COS_{(g)} + 2H^*$, $HS^* + CO_{(g)} \rightarrow COS_{(g)} + H^*$, and $S^* + CO_{(g)} \rightarrow COS_{(g)}$. The geometric configurations of Fig. 3a, b, and c are regarded as the initial state of these E-R reactions, respectively. According to the L-H mechanism, the following reaction routes are also considered: $H_2S^* + CO^* \rightarrow COS^* + 2H^*$, $HS^* + CO^* \rightarrow COS^* + H^*$, and $S^* + CO^* \rightarrow COS^*$. The geometric configurations of Fig. 2a, b, and c are regarded as the initial state of these L-H reactions, respectively.

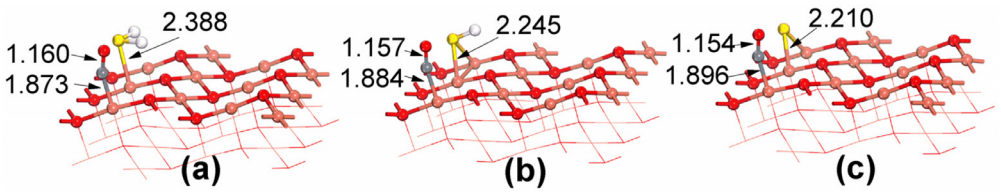

Fig. 2. The optimized configurations of co-adsorptions of (a) CO and H_2S, (b) CO and HS*, and (c) CO and S*. (Yellow ball: S, White ball: H, Red ball: O, Salmon pink ball: Cu, Grey ball: C.).

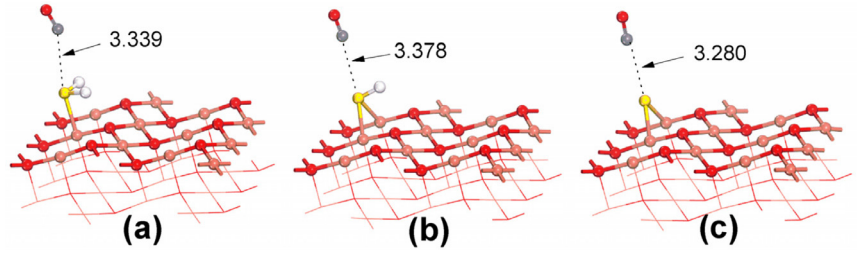

Fig. 3. The optimized configurations of CO adsorption on (a) the H_2S pre-adsorbed CuO surface, (b) the HS* pre-adsorbed CuO surface, and (c) the S* pre-adsorbed CuO surface.

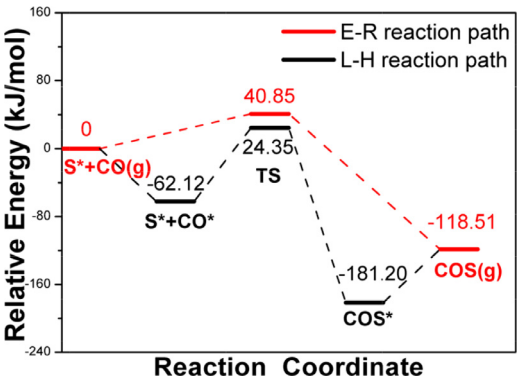

Fig. 4. The corresponding potential energy diagram for reaction of S* with CO.

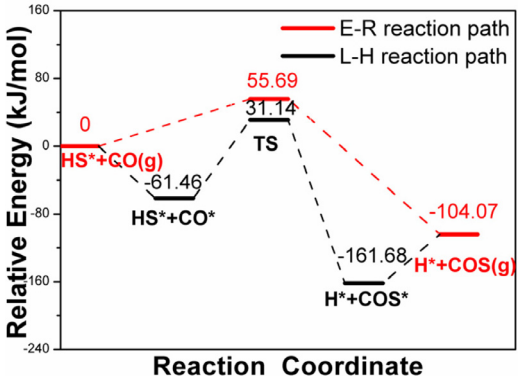

Fig. 5. The corresponding potential energy diagram for reaction of HS* with CO.

3.2.1. *CO reacts with S**

The configurations of Figs. 2c and 3c are chosen as the initial state of L-H and E-R reaction pathways, and the value of 62.12 kJ/mol in Fig. 4 is the overall energy difference of the configurations of Fig. 2c (namely 'S*+CO*' in Fig. 4) and Fig. 3c (namely '$S^*+CO_{(g)}$' in Fig. 4). As known, gaseous or adsorbed CO can react with S* to eventually produce COS. To determine the formation route of COS, all possible active adsorption sites of COS should be firstly considered (see Section S3 of SM). As shown in Fig. S7 of SM, CO prefers to migrate to the 3-coordinated oxygen site of T_{O3f} to form the adsorbed COS* (from 'S*+CO*' to 'COS*' in Fig. 4), corresponding to the L-H mechanism ($S^*+CO^*\rightarrow COS^*$). It is found that the energy barrier of the L-H reaction path is 86.47 kJ/mol. As for the E-R reaction route ($S^*+CO_{(g)}\rightarrow COS_{(g)}$), gaseous CO interacts with S* to produce COS with an energy barrier of 40.85 kJ/mol. Although the energy barrier of the L-H reaction is higher than that of the E-R reaction, the overall energy of the L-H reaction at TS (24.35 kJ/mol) is still lower than that of the E-R reaction (40.85 kJ/mol), indicating that COS is preferentially formed via the L-H mechanism between CO* and S* ($S^*+CO^*\rightarrow COS^*$).

3.2.2. *CO reacts with HS**

As it is shown in Fig. 5, the potential energy diagram for the two reaction paths between HS* and gaseous or adsorbed CO is calculated, and the corresponding configurations can be seen in Fig. S8 in SM. It is found that COS can be produced via the E-R mechanism ($HS^*+CO_{(g)}\rightarrow COS_{(g)}+H^*$) by

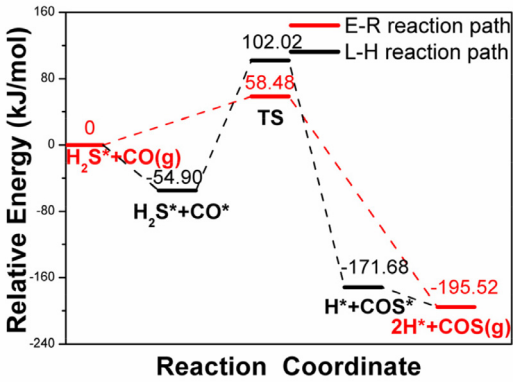

Fig. 6. The corresponding potential energy diagram for the reaction of H_2S^* with CO.

overcoming an energy barrier of 55.69 kJ/mol, while the H atom will transfer to the adjacent 3-coordinated oxygen site of T_{O3f}. As for the L-H reaction path, CO still prefers to migrate to the 3-coordinated oxygen site from 'HS^*+CO^*' to 'H^*+COS^*' in Fig. 5 with an energy barrier of 92.60 kJ/mol. Analogously, the lowest overall energy of the L-H reaction path at TS (31.14 kJ/mol) is observed, which also confirms previous speculation on the L-H mechanism between CO^* and HS^* ($HS^*+CO^*\rightarrow H^*+COS^*$).

3.2.3. CO reacts with H_2S^*

The potential energy diagram for the two reaction paths between H_2S^* and gaseous or adsorbed CO is shown in Fig. 6, and the corresponding configurations can refer to Fig. S9 in SM. The energy barrier of the E-R reaction ($H_2S^*+CO_{(g)}\rightarrow COS_{(g)}+2H^*$) is 58.48 kJ/mol, while two H^* (dissociated from H_2S) will transfer to two adjacent 3-coordinated oxygen sites. As for the L-H reaction path, due to prior occupation of H^* atoms on the 3-coordinated oxygen sites of T_{O3f}, CO can only migrate to the 4-coordinated oxygen site of T_{O4f} to produce COS^* via the reaction of $H_2S^*+CO^*\rightarrow COS^*+2H^*$. Both the energy barrier and overall energy of E-R reaction path (58.48 kJ/mol and 58.48 kJ/mol, respectively) are lower than those of the L-H reaction path (156.92 kJ/mol and 102.02 kJ/mol, respectively), which meets the initial expectation that COS are generated via the E-R reaction between CO and H_2S ($H_2S^*+CO_{(g)}\rightarrow COS_{(g)}+2H^*$).

Therefore, it can be concluded from the above calculation results that the CO/H_2S reaction mechanism changes from the E-R mechanism to the L-H mechanism as H_2S dissociation proceeds, which has already been forecasted by the co-adsorption energies and then fully verified by the results of all potential reaction paths.

3.3. H_2S dissociation and further reaction with CuO in the presence of CO

To characterize the interaction between CO and H_2S over the CuO (111) surface, the influence of CO on the H_2S dissociation process is rather essential. The potential energy diagram for H_2S dissociation and further reaction with CuO are shown in Fig. 7, in which the H_2S dissociation in the presence of CO is compared with the individual H_2S dissociation on the CuO surface [21], and the corresponding configurations can be found in Fig. S10 in SM. The co-adsorption configuration of H_2S and CO (Fig. 2a) is set as the initial state ('H_2S^*' in Fig. 7) of the H_2S dissociation process. The gradual dehydrogenations of H_2S ($H_2S^*\rightarrow HS^*+H^*$ and $HS^*\rightarrow H^*+S^*$) are firstly examined. In the first dehydrogenation step, the adsorbed H_2S^* is dissociated spontaneously into HS^* and H^* with an energy barrier of 6.66 kJ/mol at TS1, in which CO^* still binds with T_{Cu3f} site, and S^* bonds with two adjacent Cu atoms ('HS^*+H^*' in Fig. 7). Subsequently, the second dehydrogenation step occurs by overcoming an energy barrier of 39.18 kJ/mol at TS2, and as depicted in 'S^*+2H^*' in Fig. 7, the surface-adsorbed S^* is formed while two H^* adsorbs at the T_{O3f} site.

The energy barriers of the first (4.82 kJ/mol) and second (26.05 kJ/mol) steps of H_2S dehydrogenations in the absence of CO are also calculated [21]. It can be seen that, the energy barrier of the first dehydrogenation step is significantly lower than that of the second dehydrogenation step both in the presence and absence of CO, suggesting that the reaction of $HS^*\rightarrow H^*+S^*$ is the rate-determining step in the two-step dehydrogenation process. Based on the energy barrier analysis, it can be concluded that CO does not significantly affect the first H_2S dehydrogenation step (6.66 *vs.* 4.82 kJ/mol), but greatly increases the energy barrier of the second dehydrogenation step (39.18 *vs.* 26.05 kJ/mol). This indicates that the presence of CO significantly limits the dissociation of H_2S due to the increased energy barrier of the rate-determining dehydrogenation step.

In term of the reaction of $CuO+H_2S\rightarrow Cu_xS+H_2O$, the further reactions of H_2O generation and sulfur evolution are considered as a vital step to recognize the entire reaction process of the interaction of H_2S with CuO. One H^* atom is separated from the original $(O\text{-}H)^*$ group and then close to other T_{O3f} site, forming a $(H\text{-}O\text{-}H)^*$ structure with an energy barrier of 102.94 kJ/mol, which will release as $H_2O_{(g)}$ at a distance of 6 Å above the surface. This would contribute to the formation of oxygen vacancy ('$S^*+H_2O(g)$' in Fig. 7), and the desorption is endothermic (62.64 kJ/mol). According to the Lewis acid-base theory [23], the removal of an oxygen atom from CuO surface will leave behind two unpaired electrons. This implies that the

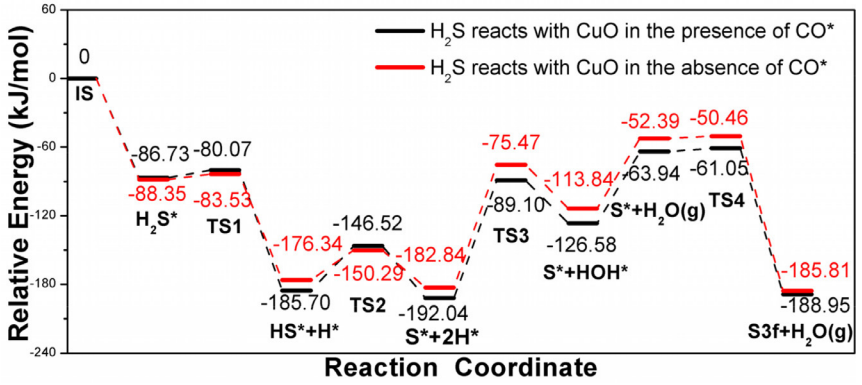

Fig. 7. The potential energy diagram for H_2S dissociation and further reaction with CuO in the presence/absence of CO.

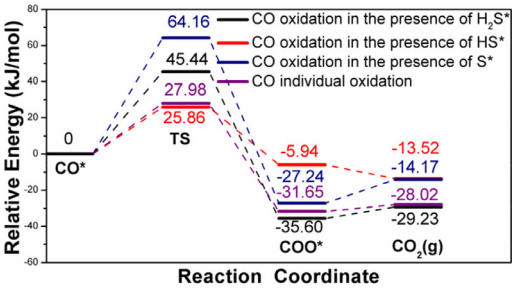

Fig. 8. The potential energy diagram for CO oxidation by CuO.

oxygen vacancy is a strong Lewis base, and the active S* will migrate to the oxygen vacancy forming a strong adsorption structure (top site of S_{3f}) in the final state ('S3f+H_2O(g)' in Fig. 7) with an energy barrier of 2.89 kJ/mol. Thus, in this sense, H_2S eventually dissociates into H_2O molecule and the residual S* remains in the surface. It is inferred that the residual S* mainly exists in the form of S_{3f} site on the CuO surface, and then lead to a generation of sulfides as more dissociated S* atoms gather. In brief, it can be concluded from Fig. 7 that CO does not significantly affect the following H_2O generation and subsequent sulfur evolution, considering their nearly same desorption energies (62.64 *vs.* 61.45 kJ/mol), and energy barriers at TS3 (102.94 *vs.* 107.37 kJ/mol) and at TS4 (2.89 *vs.* 1.93 kJ/mol).

3.4. The CO oxidation by CuO in the presence of H_2S

The impact of H_2S as well as its dissociation products on CO oxidation by CuO is also investigated, and CO oxidations in the presence/absence of H_2S*, HS*, or S* are plotted in Fig. 8. The corresponding configurations are shown in Fig. S11 in SM. It is noted that CO interacts with the surface oxygen, forming a surface linear CO_2 complex which bonds with copper atom, leading to the release of gaseous CO_2. The energy barriers of CO oxidation in the presence of H_2S* or S* are 45.44 and 64.16 kJ/mol, respectively, and both of which are obviously higher than that of CO individual oxidation (27.98 kJ/mol), indicating that the sulfur presence significantly restrains the CO oxidation. In addition, there is little difference of the reaction energy among the above three reactions. However, in the presence of HS*, the CO oxidation is nearly unaffected (their almost identical energy barriers). Furthermore, the release of CO_2 with the presence of HS* is exothermic (−7.58 kJ/mol), which is entirely different from the above endothermic desorption of CO_2. In conclusion, the oxidation reactivity of CO with CuO in the presence of H_2S* or S* would greatly decrease, while the presence of HS* contributes to the highest oxidation activity of CO.

3.5. Competitive interaction mechanism among CuO, CO, and H_2S

Based on the above results, the competitive potential energy profiles of the interaction mechanisms of H_2S and CO over CuO surface are concluded. As it is shown in Fig. 9, the black line represents the H_2S dissociations on the CuO surface in the presence of CO, and the red lines represent the formation of COS. It should be noted that the COS formation adopts the most favorable reaction mechanism as determined in Section 3.2, *i.e.*, $CO_{(g)}$+H_2S* (the E-R mechanism), CO*+HS* (the L-H mechanism), and CO*+S* (the L-H mechanism). It can be observed in Fig. 9 that three stages of the H_2S dissociation exhibit thoroughly different performance on the reaction paths.

Firstly, in the stage of H_2S and CO, adsorbed H_2S* would prefer to dissociate into HS* and H* for its lowest energy barrier (6.66 kJ/mol), while the COS formation is rather difficult to occur even via the E-R reaction, for its quite higher overall energy barrier. Next, in the stage of 'HS*+H*+CO*' in Fig. 9, COS is also difficult

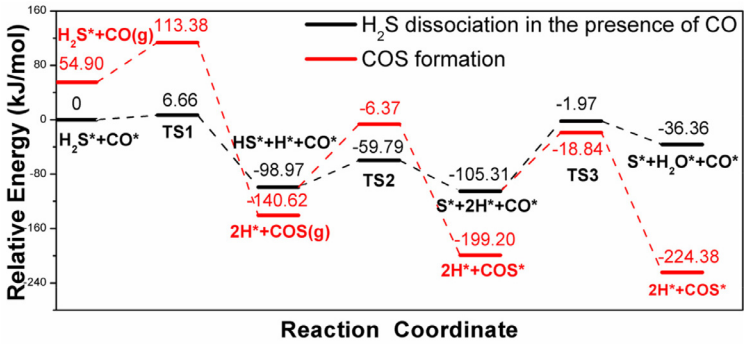

Fig. 9. The complete potential energy profiles of interaction mechanisms among CuO, CO, and H_2S.

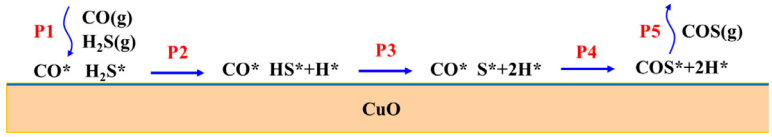

Fig. 10. Comprehensive interaction mechanisms among CuO, CO, and H_2S.

to generate; however, the overall energy of COS formation dramatically reduces, and the generation of COS is promoted to some extent. In this stage, the dissociated HS* would still prefer to dissociate into S* and H*. Finally, in the stage of 'S*+2H*+CO*' in Fig. 9, two H* will undergo a H_2O-formation process (with an energy barrier of 102.94 kJ/mol for 'S*+H_2O*+CO' at TS3) and leave an oxygen vacancy, which is beneficial for the subsequent sulfur evolution. However, the energy barrier of 86.47 kJ/mol is just required to produce COS via the L-H mechanism, implying that the COS formation is easier than the H_2O-elimination and the generation of S_{3f}, as well as sulfidation reaction and oxygen carrier poisoning. Therefore, COS is more preferentially produced over the CuO surface via the L-H reaction between the active surface S* and CO*, which is in line with previous DFT results [13].

The comprehensive interaction mechanisms among CuO, CO, and H_2S are summarized in Fig. 10. As it can be seen, under a reductive reactive atmosphere, H_2S and CO always coexist and co-adsorb on the CuO (111) surface. Then, H_2S prefers to dissociate into two H* and one S* on the CO pre-adsorbed surface, and COS will be produced via the L-H reaction between the active S* and CO*, which can well explain the COS formation in experiments [8,9]. As indicated by Fig. 7, the dissociations of H_2S will lead to the generation of residual S* (S_{3f}) on the CuO surface. Meanwhile, when looking into the pathways of SO_2 formation via the reaction between S_{3f} and surface lattice oxygen, it is found that S_{3f} favors to exist on the surface rather than the SO_2 formation in the absence of gaseous O_2, and copper sulfides will generate as the dissociation of H_2S proceeds and more S_{3f} atoms gather on the CuO (111) surface [21]. In other words, under an O_2-free and CO-rich condition, the formation of COS, SO_2, and Cu_xS follows this order of COS> Cu_xS >SO_2. However, it is noted that the reaction reactivity between COS and fresh CuO surface is kinetically and thermodynamically unfavorable [21]. To effectively complete the sulfur fixation and control sulfur emission, it is possible to develop a composite material by doping different metal or nonmetallic oxide compounds into the Cu-based oxygen carrier. In this sense, gaining insights into the intrinsic interaction and reaction mechanism/kinetics of H_2S or CO over Cu-based oxygen carrier at a microcosmic level is critical to reveal the sulfur fate in the realistic chemical-looping system, as well as to rationally design high-performance Cu-based oxygen carrier.

4. Conclusions

In this study, DFT calculations are performed to investigate the interaction mechanisms among H_2S, CO, and CuO. The main conclusions are drawn as follows:

(1) Based on the adsorption results, it is found that H_2S (or HS*, S) will preferentially chemisorb on the CuO (111) surface. The co-adsorption results imply that the reaction between CO and H_2S is more likely to occur to produce COS via the E-R reaction, while CO prefers to react with HS* or S* via the L-H reaction, suggesting that the reaction mechanism changes as the H_2S dissociation proceeds, which has already been forecasted by

the co-adsorption energies and then verified by the calculation results of all potential reaction pathways.

(2) As for the impact of CO on the H_2S dissociation and further reaction, the presence of CO limits the dissociation of H_2S to a large extent due to the increased energy barrier of the rate-determining step in the two-step dehydrogenation steps, but does not significantly affect further H_2O generation and subsequent sulfur evolution.

(3) In term of the impact of H_2S dissociation products on CO oxidation with CuO, it is found that the rate-limiting step of CO oxidation is the activation of surface oxygen, instead of the desorption of CO_2. The oxidation activity of CO with CuO in the presence of H_2S^* or S^* will greatly decrease, while the presence of HS^* contributes to the highest CO oxidation activity.

(4) The competitive potential energy profiles of the interaction mechanism among H_2S, CO, and CuO are concluded. It is found that H_2S will prefer to dissociate into HS^* and H^* at the very initial stage, and COS will be inevitably produced over the CuO surface via the L-H reaction between active S^* and CO^*, which is prior to further H_2O generation and subsequent sulfidation of Cu-based oxygen carrier.

Declaration of Competing Interest

The authors declare no competing financial interest.

Acknowledgements

This work was founded by "National Key R and D Program of China (No. 2016YFB0600801)".

Supplementary materials

Supplementary material associated with this article can be found, in the online version, at doi:10.1016/j.proci.2020.06.260.

References

[1] A. Nandy, C. Loha, S. Gu, P. Sarkar, M.K. Karmakar, P.K. Chatterjee, *Renew. Sust. Energ. Rev* 59 (2016) 597–619.
[2] H. Zhao, X. Tian, J. Ma, M. Su, B. Wang, D. Mei, *Int. J. Greenh. Gas Con.* 93 (2020) 102898.
[3] S.Y. Chuang, J.S. Dennis, A.N. Hayhurst, S.A. Scott, *Combust. Flame* 154 (1) (2008) 109–121.
[4] J. Ma, C. Wang, H. Zhao, X. Tian, *Energ. Fuel* 32 (4) (2018) 4493–4501.
[5] I. Adánez-Rubio, A. Abad, P. Gayán, F. García-Labiano, L.F. de Diego, J. Adánez, *Appl. Energ.* 113 (2014) 1855–1862.
[6] X. Tian, K. Wang, H. Zhao, M. Su, *Proc. Combust. Inst.* 36 (3) (2016) 3381–3388.
[7] R.F. Pachler, K. Mayer, S. Penthor, M. Kollerits, H. Hofbauer, *Int. J. Greenh. Gas Con.* 71 (2018) 86–94.
[8] C.R. Forero, P. Gayán, F. García-Labiano, L.F. de Diego, A. Abad, J. Adánez, *Int. J. Greenh. Gas Con.* 4 (5) (2010) 762–770.
[9] K. Wang, X. Tian, H. Zhao, *Appl. Energ.* 166 (2016) 84–95.
[10] H. Yang, R. Sothen, D.R. Cahela, B.J. Tatarchuk, *Ind. Eng. Chem. Res.* 47 (24) (2008) 10064–10070.
[11] W. Xie, L. Chang, D. Wang, K. Xie, T. Wall, J. Yu, *Fuel* 89 (4) (2010) 868–873.
[12] J. Yu, L. Chang, W. Xie, D. Wang, *Korean J. Chem. Eng.* 28 (4) (2011) 1054–1057.
[13] L. Ling, Z. Zhao, B. Wang, M. Fan, R. Zhang, *Phys. Chem. Chem. Phys.* 18 (16) (2016) 11150–11156.
[14] L. Tao, X. Guo, C. Zheng, *Proc. Combust. Inst.* 34 (2) (2013) 2803–2810.
[15] H.F. Wang, R. Kavanagh, Y.L. Guo, Y. Guo, G. Lu, P. Hu, *J. Catal.* 296 (12) (2012) 110–119.
[16] B. Yang, L. Ye, H. Gu, J. Huang, H. Li, Y. Luo, *J. Mol. Model.* 21 (8) (2015) 195.
[17] S. Sun, D. Zhang, C. Li, Y. Wang, *RSC Adv.* 5 (28) (2015) 21806–21811.
[18] J. Zhang, M. Liu, R. Zhang, B. Wang, Z. Huang, *Mol. Catal.* 438 (2017) 130–142.
[19] J.P. Perdew, J.A. Chevary, S.H. Vosko, K.A. Jackson, M.R. Pederson, D.J. Singh, et al., *Phys. Rev. B* 46 (11) (1992) 6671–6687.
[20] M. Su, J. Cao, X. Tian, Y. Zhang, H. Zhao, *P. Combust. Inst.* 37 (2019) 4371–4378.
[21] C. Zheng, H. Zhao, *Fuel Process. Technol.* 205 (2020) 106431.
[22] V. Massarotti, D. Capsoni, M. Bini, A. Altomare, A.G.G. Moliterni, *Z. Kristallogr.* 213 (5) (1998) 259–265.
[23] J. Paier, C. Penschke, J. Sauer, *Chem. Rev.* 113 (6) (2013) 3949–3985.